Exploration of Decadal Tidal Evolution in Response to Morphological and Sedimentary Changes in the Yangtze Estuary

Zhu, Chunyan; Guo, Leicheng; van Maren, D. S.; Wang, Zheng Bing; He, Qing

Important note
To cite this publication, please use the final published version (if applicable).
Please check the document version above.

Exploration of Decadal Tidal Evolution in Response to Morphological and Sedimentary Changes in the Yangtze Estuary

Chunyan Zhu[1,2] , Leicheng Guo[1] , D. S. van Maren[1,2,3], Zheng Bing Wang[1,2,3] , and Qing He[1]

[1]State Key Lab of Estuarine and Coastal Research, East China Normal University, Shanghai, China, [2]Faculty of Civil Engineering and Geosciences, Delft University of Technology, Delft, The Netherlands, [3]Deltares, Delft, The Netherlands

Abstract Estuarine tidal dynamics are influenced by changes in morphology and friction. In this work, we quantified changes in tidal damping in the Yangtze Estuary and explored the impact of morphology and friction using a numerical model. In-depth analyses of tidal data reveal a strong reduction in tidal damping from 1990 to 2010, followed by a slightly enhanced damping from 2010 to 2020 in the South Branch. The reduced tidal damping in the South Branch from 1990 to 2010 is controlled by sediment decline which induces an increase in water depth (erosion), thereby strongly amplifying tides. However, the effective bottom roughness (Manning coefficient) is increased by 60%, which is probably related to the ~80% decrease in the suspended sediment concentration (SSC). Such an effect may enhance tidal damping, which counteracts the contribution of water depth increase on amplifying tides by ~75%. From 2010 to 2020, the tides in the South Branch became more damped, suggesting a dominance of the decrease in SSC over the morphological changes. In the mouth zone, tidal dissipation is enhanced from 1997 to 2010, which is mainly caused by an overall increase in effective bottom roughness. Local structures dominate the increase in effective bottom roughness; however, fluid mud formation may contribute to a decrease after 2010. Overall, we argue that estuarine morphological and sedimentary changes in response to riverine sediment decline and local engineering works control the tidal evolution in the Yangtze Estuary, which is important for evaluation of human activities and estuarine management.

Plain Language Summary In many estuaries, human interventions have strongly influenced bed levels and sedimentary features (e.g., sediment concentration, sediment grain size), which led to consequent changes in tidal dynamics. In this study, we investigated decadal changes in the tidal propagation in the Yangtze Estuary from field data and explored the mechanisms responsible for these changes using a numerical model. This study suggests that tidal damping is weakened in the South Branch and enhanced in the mouth zone of the Yangtze Estuary. Local structures enhance tidal damping, whereas a reduction in riverine sediment supply has a more complex response by influencing bed roughness and bed levels. These findings are important for understanding and management of morphodynamic changes in strongly engineered estuaries.

1. Introduction

Anthropogenic activities may strongly influence the morphology in varying coastal environments, particularly in tidal estuaries where hydro-morphodynamic feedback processes are important. Human interventions potentially influence tidal dynamics, in terms of tidal range, amplitudes, and wave shape, resulting in tidal amplification/damping, and deformation. These modifications in turn influence the intertidal area, salinity and freshwater availability, as well as the navigational depth. A thorough understanding of changes in tidal amplification/damping is therefore crucial for sustainable coastal management.

Tidal amplitudes and ranges have been observed to increase in many estuaries owing to channel deepening related to dredging (Talke & Jay, 2020; Woodworth, 2010). For instance, on the U.S. East Coast, the mean tidal range in the Cape Fear River Estuary in Wilmington (NC) had doubled to 1.55 m since the 1880s (Familkhalili & Talke, 2016). In Ria de Aveiro, Spain, an averaged increase of 0.245 m in the M_2 amplitude and an averaged 17.4° decrease in the M_2 phase were detected over 16 years (1987–2004) (Araújo et al., 2008). The amplitudes of the major tidal constituents exhibited a significant increase over the last

century in the Venice Lagoon (Ferrarin et al., 2015). The tidal range in the upstream reaches of the Hudson River had more than doubled over 150 years (Ralston et al., 2019). Interestingly, decreases in tidal amplitudes are less documented, except in a few studies such as in Norfolk, Virginia; Washington DC; and Providence, Rhode Island where the mean tidal range has decreased by 8%–9% since the mid-nineteenth century (Talke & Jay, 2020). Moreover, a decrease in tidal amplitude is found in the Yangshan Harbour and Yalu river estuary due to the dams and land reclamation (Cheng et al., 2020; W. Guo, Wang, et al., 2018).

Tidal amplitudes and ranges are strongly dependent on morphology, particularly on changes in water depth and channel width. Increasing water depth reduces the effects of bottom friction, causing a reduction in the effective hydraulic drag, resulting in an increase in amplitude and propagation speed of tidal waves (Ralston et al., 2019). The increase in tidal amplitude in many estuaries is found to be caused by the increase in water depth, some of which are caused by natural morphological changes (Jalón-Rojas et al., 2018) while others are associated with human-induced dredging activities, such as in the Rhine-Meuse Delta (Vellinga et al., 2014), Tampa Bay (J. Zhu et al., 2015); Elbe Estuary, Ems Estuary, and Loire Estuary (Winterwerp et al., 2013), upper Scheldt estuary (Z. B. Wang et al., 2019), Columbia Estuary (Jay et al., 2011), and Cape Fear River Estuary (Familkhalili & Talke, 2016).

The deepening of tidal channels usually results in a modification of both vertical and horizontal tides. Enlarged tidal currents lead to an increase in SSCs (de Jonge et al., 2014; Dijkstra, Schuttelaars, Schramkowski, & Brouwer, 2019). High SSCs cause a reduction in the effective hydraulic drag due to buoyancy destruction (Winterwerp et al., 2009), which in turn cause a stronger tidal amplification in estuaries (Gabioux et al., 2005; Jalón-Rojas et al., 2016, 2018; Winterwerp & Wang, 2013; Winterwerp et al., 2013; Z. B. Wang et al., 2014). A positive feedback was identified between channel deepening, increase in SSCs, reduction in bottom drag, and enhanced tidal amplification, which increases sediment trapping and SSC, and potentially induce a regime shift to hyper-turbid conditions (Dijkstra, Schuttelaars, & Schramkowski, 2019; Dijkstra, Schuttelaars, Schramkowski, & Brouwer, 2019; Winterwerp, 2011; Winterwerp & Wang, 2013; van Maren et al., 2015). This phenomenon has been documented for the Ems (de Jonge et al., 2014; Dijkstra, Schuttelaars, & Schramkowski, 2019; Dijkstra, Schuttelaars, Schramkowski, & Brouwer, 2019), and Loire estuaries (Winterwerp et al., 2013). In contrast, a decline in SSC owing to a reduction in sediment availability from the upstream watershed may increase bottom drag and affect tidal dynamics, which is probably the case of the Yangtze Estuary.

The Yangtze Estuary is a large-scale alluvial system undergoing changes within the estuary and at the boundary, driven by intensive human activities. The estuary is a highly turbid system with near-bottom SSC up to 100 kg/m^3, forming near-bed fluid mud in the mouth zone (Wan, Roelvink, et al., 2014). The high SSC has a damping effect on the turbulence and thereby decreases the effective bed roughness (Geyer, 1993; Winterwerp et al., 2009). As a result, a very low friction parameter (e.g., a Manning coefficient n of 0.012 s/m$^{1/3}$, Hu et al., 2009) is needed to correctly simulate tidal wave propagation in the Yangtze Estuary. It is likely, however, that the effect of sediment on the bed roughness is changing over time. On the one hand, an increase in fluid mud thickness has been observed in the North Passage of the Yangtze Estuary (G. Liu et al., 2011; Song et al., 2013; Wan, Roelvink, et al., 2014), owing to enhanced stratification after the construction of the jetties and groins. This change potentially reduces the regional bed roughness. On the other hand, dam construction in the river basin causes a drastic decline in river-borne sediment supply since 2003 (L. Guo, Su, et al., 2018; Luan et al., 2016; S. L. Yang et al., 2011; Zhao et al., 2018). As a result, the SSC in the Yangtze Estuary decreases accordingly in recent decades, although the degree of this reduction varies spatially (H. Liu, 2009; W. Zhu et al., 2015). Vertical SSC gradients dampen vertical mixing, leading to a hydraulically smoother bed (Winterwerp, 2001; Winterwerp et al., 2009; van Maren et al., 2015). Therefore, a reduction in SSC is expected to strengthen bottom friction and subsequently deform the tidal wave. Additionally, the morphology of the Yangtze Estuary is changing as well. The construction of long jetties and a series of groins to regulate the navigational waterway, together with intensive dredging and land reclamation, has modified the estuarine morphology substantially. These human interventions influence the hydrodynamics (e.g., Hu & Ding, 2009; L. Zhu et al., 2018) in the short term and morphological changes in the long term (e.g., Jiang et al., 2012; Zhao et al., 2018; C. Zhu et al., 2019). Our understanding of the tidal dynamics in the Yangtze Estuary is progressively increasing in recent years concerning the temporal and spatial variations of tidal dynamics (Fu, 2013; Lu et al., 2015; Wan, Gu, et al., 2014) and river-tide interactions (Cai et al., 2014;

L. Guo et al., 2015). However, to what degree the tides in the Yangtze Estuary have changed in response to the various human interventions remains insufficiently known.

In this contribution, we aim to examine the decadal changes in the tidal dynamics of the Yangtze Estuary using observational data and subsequently unravel the role of changes in morphology, sediment concentration and human interventions using a numerical model. The structure of this paper is as follows. The study area is described first, followed by an overview of available data and setup of the model and model scenarios. In the results section, we introduce the observed and computed tidal evolution, whereas the mechanisms contributing to this tidal evolution are interpreted in the discussion. We finalize with conclusions.
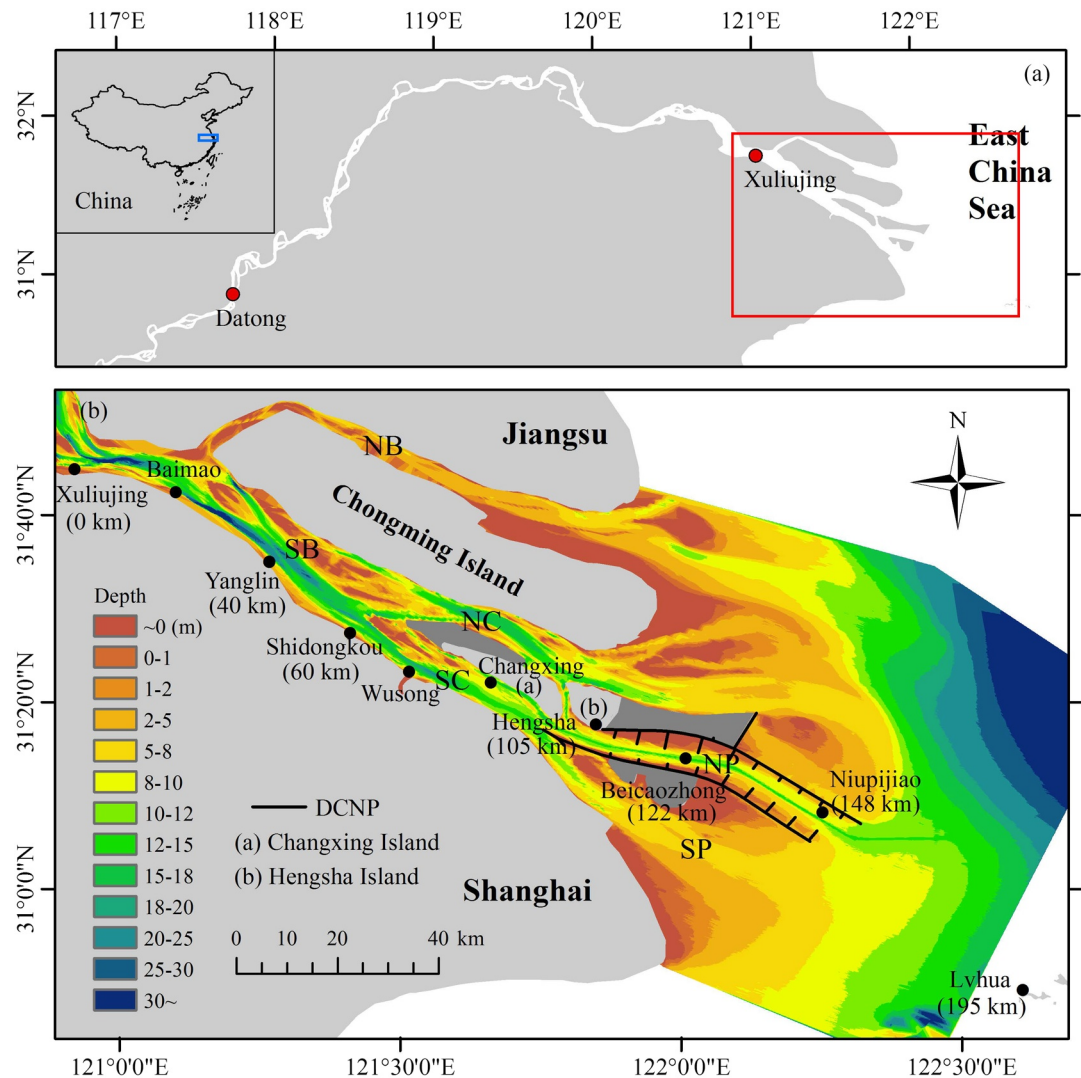
2. Study Area

The Yangtze River is one of the largest rivers in the world in terms of its river length (~6,300 km) and catchment area (~1.9 million km^2). Datong station, ~490 km upstream of Xuliujing, is the tidal wave limit in the dry seasons. The yearly mean river discharge monitored at Datong is 28,200 m^3/s (1951–2016), but monthly averaged values fluctuate between 10,000 and 80,000 m^3/s. The annual suspended sediment load has declined from 424 million tons per year (1951–2002) to 134 million tons per year (2003–2018). The river flows south-eastward into the East China Sea via its four outlets in the Yangtze Estuary, that is, the North Branch, the North Channel, the North Passage, and the South Passage (Figure 1). In this work, we mainly focus on the inner South Branch and the seaward mouth zone including the North Channel, North Passage, and its seaward area. Xuliujing station, the bifurcation point between the North Branch and the South Branch, is defined as the origin ($x = 0$ km) of the axis. Tides in the Yangtze Estuary have a predominantly semi-diurnal regime with a form factor $(A_{O1} + A_{K1})/(A_{M2} + A_{S2})$ ranging between 0.15 and 0.25 (Lu et al., 2015; Yun, 2004) and the oceanic tides show no long-term changes other than the nodal tidal variations. In the landward direction, tidal waves are first slightly amplified from offshore to the nearshore (up to Niupijiao) owing to decreased water depth, and then predominantly damped further inside the estuary owing to the combined effect of bed friction and river discharge (L. Guo et al., 2015). The seasonal variations in tidal amplitude in the region upstream of Xuliujing are dominantly controlled by highly nonstationary river discharge.

In the past 60 years, both the reduction in riverine sediment input and large-scale human interventions influence the hydro-morphodynamics in the Yangtze Estuary. The annual river discharge at Datong has remained stable since 1954, but its seasonal variations are regulated by hydropower dams, that is, increased river discharges in the dry season and reduced peak river discharges in the wet season (L. Guo, Su, et al., 2018). The suspended sediment load has gradually decreased since the mid-1980s, and this reduction has accelerated since 2003 when the TGD began operation (L. Guo, Su, et al., 2018; Luan et al., 2016; S. L. Yang et al., 2011; Zhao et al., 2018). Within the estuary, the Deep Channel Navigation Project (DCNP) was implemented in the North Passage from 1997 to 2010 with three phases (Figure 2). Phase I of the project (1998–2001) involved the construction of diversion works at the bifurcation between the North and South Passage, of the northern training jetty and groins (N1–N5), and the southern training jetty and groins (S1–S5). The navigation channel was deepened to 8.5 m with a 300 m width. Phase II of the project was undertaken between 2002 and 2005, including the extension of the two training jetties and construction of the groins N6–N10 and S6–S9. The navigational channel was deepened, reaching a depth of 10 m and a width of 300–400 m. Phase III of the project was carried out from 2006 to 2010, during which the navigational channel was deepened to 12.5 m with the construction of a 21-km long sediment-retention jetty and lengthening of the groins. Between 2007 and 2016, an average of 72 million m^3 of sediment was annually dredged along the North Passage, of which approximately 30% was disposed on Hengsha flat to create land, and the remaining parts were disposed partly in the shallow areas between the groins and partly offshore (C. Zhu et al., 2019).

3. Material and Methods

3.1. Data

Long time series of river discharges, sediment loads, and water levels in the Yangtze Estuary were provided by the Bureau of Hydrology, Changjiang Water Resources Commission (CWRC) for detailed analysis. Daily

Figure 1. (a) The Yangtze Estuary and (b) the study area and the tidal gauge stations. The figures in brackets are distances downstream of Xuliujing ($x = 0$ km). DCNP: Deep Channel Navigation Project. NB: North Branch; NC: North Channel; NP: North Passage; SB: South Branch; SC: South Channel; SP: South Passage.

river discharges between 1958 and 2020 and annual sediment loads between 1951 and 2019 were collected at Datong. Hourly tidal water levels were provided for 1990–1991, 2009–2010, and 2019–2020 at Xuliujing and Yanglin ($x = 40$ km) to reveal the tidal evolution in the South Branch. In addition, the yearly averaged tidal ranges are obtained from the yearly averaged high and low water levels from 1996 to 2011 (Fu, 2013) at seven stations, that is, Shidongkou ($x = 60$ km), Wusong ($x = 70$ km), Changxing, Hengsha ($x = 105$ km), Beicaozhong ($x = 122$ km), Niupijiao (except in 1996–2001) and Lvhua to quantify the decadal tidal evolution in the mouth zone. Time series of hourly water levels are available at Xuliujing and Wusong between 2006 and 2015.

Bathymetric data are available for 1986, 1997, 2002, 2007, 2010, and 2016; see C. Zhu et al. (2019) for details of the digitalization, accuracy, and description of the bathymetry maps. These bathymetries are further used to explore the effect of morphological changes using a numerical model.
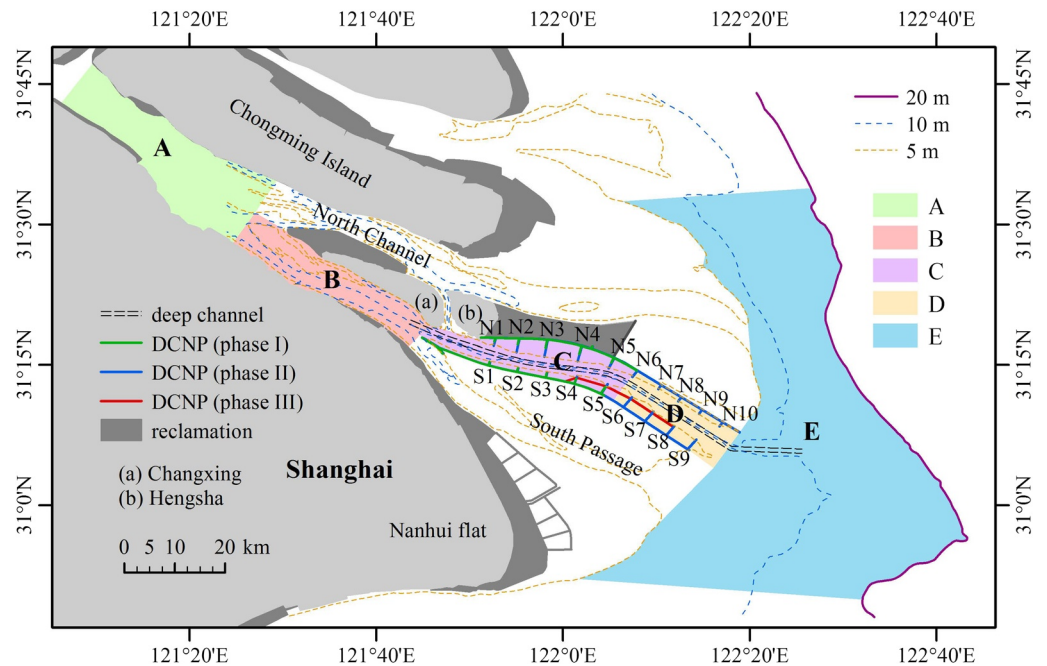
Figure 2. The three phases of the Deep Channel Navigation Project (DCNP), reclamation areas and the regions A, B, C, D, and E in the Yangtze Estuary.

3.2. Data Analysis

Tidal evolution is evaluated by changes in tidal amplitudes and ranges, phases, and tidal damping factors. The amplitudes and phases of the main tidal constituents are determined by harmonic tidal analysis with nodal corrections, by using the t-tide function (Pawlowicz et al., 2002). To evaluate the effect of seasonal river discharge variations, we also employed an enhanced harmonic analysis for nonstationary tides using the s-tide function to resolve the main tidal constituents (Pan et al., 2018; D. Wang et al., 2020).

To eliminate natural tidal amplitude variations over time, we define a damping factor per section of the estuary to quantify the amplification/damping rate of the tidal waves. Note that the damping factor shows spring-neap variations as tidal dissipation is stronger in spring tides than neap tides; however, the change is negligible in decadal tidal analysis. A damping factor is the ratio of tidal range in the landward station to a more seaward station, equivalent to the amplification factor (see Jalón-Rojas et al., 2018; Z. B. Wang et al., 2014, 2019). The tidal ranges are estimated similar to Kukulka and Jay (2003) and Matte et al. (2013), by high-pass filtering the hourly water levels to remove variations at subtidal frequencies, interpolating the data to 6 min intervals, and determining the minimum and maximum heights using a 25 h moving window with a 1 h time step (L. Guo et al., 2015). We additionally compute the hydraulic head, which strongly depends on the river discharge but provides indications for changes in morphology (e.g., the water depth, storage width, and hydraulic drag, see Z. B. Wang et al., 2019). For a given time series of water levels, for example, at Xuliujing and Yanglin, the hydraulic head is determined as the difference between the subtidal water levels at Xuliujing and Yanglin.

3.3. Numerical Modeling

3.3.1. Model Setup

Since both morphology and SSC affect tidal amplification, it is technically difficult to identify the different controlling variables based on observations only. In numerical models, the contribution of morphological changes can be evaluated from simulations using historic bathymetries under the same forcing conditions (Grasso & Le Hir, 2019; Lopes et al., 2013). The effect of SSC changes on the tides on a decadal scale can be evaluated by varying bed roughness, for example, the Manning coefficient n (van Maren et al., 2015; Z.

B. Wang et al., 2014). Note that the bed roughness in numerical models is a combined result of bedforms, subgrid-scale morphology, near-bed turbulence, bed properties, and vegetation, and so on. For instance, the apparent bed roughness is smaller in three-dimensional (3D) baroclinic models than two-dimensional (2D) models in case of suppression of turbulence near the bed resulting from steep concentrations or vertical salinity gradients induced by salinity or sediments (Winterwerp et al., 2009). Therefore, we developed a 2D barotropic model in which salinity but especially the role of sediments is parameterized in the bed roughness. The contribution of morphology, construction of structures, and bed roughness can then be evaluated individually. The required modifications in the bed roughness are subsequently interpreted in terms of changes in SSC and fluid mud occurrences.

In addition, the Yangtze Estuary is such a large estuary that patterns of tidal amplification/damping (and underlying mechanisms leading to these tidal changes) may vary spatially. Therefore, in this study, we quantify the decadal tidal evolution with the damping factor in different parts of the estuary based on water level data since the 1990s. The numerical model is subsequently applied to interpret the physical mechanisms responsible for the observed changes using historic bathymetries in 1986, 1997, 2002, 2007, 2010, and 2016.

The model was set up using the Delft3D model system (Lesser et al., 2004), which simulates flow, sediment transport, and morphological changes. The 2D model is simulated for a full year in 2006 to reach equilibrium and another full year in 2007 for further study with realistic forcing of river discharges measured at Datong. The jetties and groins in the North Passage (since 1998) are numerically implemented as structures completely blocking through- or overflow. The effect of the hydraulic drag is expressed in terms of the Manning coefficient n (s/m$^{1/3}$) which is initially converted from existing values of the Nikuradse roughness length varying from 0.002 to 0.008 m (L. Zhu et al., 2016) and the water depth:

$$n = h^{\frac{1}{6}} \Bigg/ \left[18 \log \left(\frac{12\,h}{k_s} \right) \right]$$

Where h is the water depth (m), k_s is the Nikuradse roughness length (m). The resulting Manning coefficient n (s/m$^{1/3}$) is then calibrated ranging from 0.013 to 0.022. Note that the Manning coefficient n is so frequently used in this study that the unit is hereafter omitted. The Manning coefficient n (the reference n in Table 1) is relatively small in the estuary (0.013 ~ 0.018) and high in the river upstream of $x = 0$ km (0.018 ~ 0.022) as well as seaward of $x = 195$ km (0.018 ~ 0.02).

3.3.2. Model Calibration

The model is calibrated against measured water levels for the whole year of 2007. The computed water level at the eight stations agrees well with the measured data exemplified with August–September 2007 (see Figure S1). Both the modeled M$_2$ amplitude and tidal range are consistent with the observations from August 15, 2007 to September 15, 2007 (Figures 3a and 3b). From the mouth (Lvhua) to its upstream, the tides are amplified by 8% to $x = 148$ km and then damped by 30% further upstream. For the M$_2$ constituent, the difference between the computed and measured amplitudes is less than 5%. Similarly, the difference between observed and modeled tidal ranges in the same period is also less than 5%. For a whole year, we computed tidal ranges at nine stations (see Figure 1), to compare with the measurements (Figure 3c). We also calibrated damping factors in the reaches Xuliujing-Yanglin, Shidongkou-Hengsha, Hengsha-Beicaozhong, Beicaozhong-Niupijiao, Hengsha-Niupijiao, Niupijiao-Lvhua, and Hengsha-Lvhua (Figure 3d). The differences between the modeled and observed yearly averaged tidal ranges as well as damping factors are less than 5%. This calibration suggests a high-performance level of the numerical tidal model which is subsequently used to study the impact of changing boundary conditions.

3.3.3. Model Scenarios

Three groups of simulations were executed (Table 1), based on the changes in topography (hindcast scenarios) and friction coefficients (as a sensitivity test and for detailed calibration):

1. Historic scenarios ("tpg1"–"tpg6") are executed for the years 1986, 1997, 2002, 2007, 2010, and 2016 with different phases of jetties and groins constructed in 2002 (phase I), 2007 (phase I and II), 2010 (phase I and II) and 2016 (phase I and II). This group accounts for the effect of topography (including

Table 1
List of Scenarios Implemented in the Model

Aim	Cases	Depth	Local structures (phase)	Roughness	Note
Sensitivity to topography	"tgp1"	1986	-	Reference	-
	"tgp2"	1997	-	Reference	-
	"tgp3"	2002	I	Reference	-
	"tgp4"	2007	I & II	Reference	Calibrated
	"tgp5"	2010	I & II	Reference	-
	"tgp6"	2016	I & II	Reference	-
Sensitivity to roughness	"rgh0"	2007	I & II	Reference	Calibrated
	"rgh1"	2007	I & II	0.9A	-
	"rgh2"	2007	I & II	0.9B	-
	"rgh3"	2007	I & II	0.9C	-
	"rgh4"	2007	I & II	0.9D	-
	"rgh5"	2007	I & II	0.9E	-
Optimize roughness	"cal_tgp1"	1986	-	0.75A	Recalibrated
	"cal_tgp2"	1997	-	1.1B0.75(CDE)	Recalibrated
	"cal_tgp3"	2002	I	1.2B0.8D0.7E	Recalibrated
	"cal_tgp4"	2007	I & II	Reference	Calibrated
	"cal_tgp5"	2010	I & II	1.2(ABC)0.7E	Recalibrated
	"cal_tgp6"	2016	I & II	1.25A	Recalibrated
	"cal_mor1"	1986	-	0.75A	Recalibrated
	"cal_mor2"	1997	-	1.1B0.75(CDE)	Recalibrated
	"cal_mor3"	2002	-	1.2B1.3C0.8D0.7E	Recalibrated
	"cal_mor4"	2007	-	1.1C0.9D0.9E	Recalibrated
	"cal_mor5"	2010	-	1.2(AB)1.3C0.9D0.7E	Recalibrated
	"cal_mor6"	2016	-	1.25A	Recalibrated

Note. Local structures of phase I include jetties and groins (N1–N5, S1–S5) whereas phases I & II include N1–N10 and S1–S9 (see Figure 2). "0.9A," "0.9B," "0.9C," "0.9D," and "0.9E" represent a 10% decrease in the Manning coefficient n in the regions A, B, C, D, and E, respectively (see Figure 2) compared with the reference roughness in the calibrated case, similarly for the roughness in the other series.

the morphological changes and the simulated engineering structures) on tidal evolution. To reveal the effect of bathymetry (and also roughness hereafter), all scenarios are run with the same river discharge, using the hydrograph of the year 2007. The sensitivity of tidal damping to the river discharged will be evaluated in more detail in the discussion.

2. The sensitivity of tidal dynamics to effective bottom roughness is explored with runs "rgh0"–"rgh5." The effective bottom roughness is lowered to estimate the effect of fluid mud formation in the North Passage (following e.g., van Maren et al., 2015; Z. B. Wang et al., 2014; Winterwerp et al., 2013). We use a reduction of 10% to account for a reduced sediment supply (which is less than the 15%–50% change introduced by the studies mentioned above). The effect of a 10% decrease in Manning coefficient n was evaluated for regions A, B, C, D, and E (see Figure 2), named "0.9A," "0.9B," "0.9C," "0.9D," and "0.9E," respectively.

3. The last group was calibrated to observed amplification/damping by changing the bed roughness in the historic scenarios, with ("cal_tpg1"–"cal_tpg6") and without ("cal_mor1"–"cal_mor6") the effect of local structures. This calibration was executed by iteratively modifying the roughness in parts of the model domain (using the "rgh" series as an initial estimate) to fit modeled tidal damping factors to the observed tidal damping factors. The comparison between the simulations with and without local structures also indicates the effect of local structures on the calibrated roughness changes.
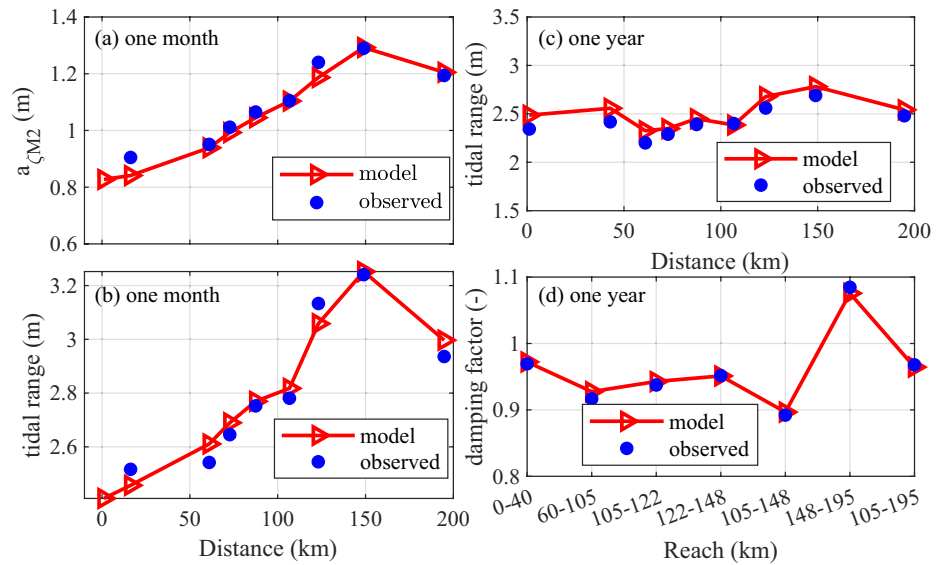
Figure 3. Comparison between observed and modeled (a) M_2 amplitude ($a_{\zeta M2}$) during 15 August–September 15, 2007; (b) tidal range during 15 August–September 15, 2007; (c) yearly averaged tidal range in 2007; and (d) yearly averaged damping factor in the reaches Xuliujing-Yanglin (0–40 km), Shidongkou-Hengsha (60–105 km), Hengsha-Beicaozhong (105–122 km), Beicaozhong-Niupijiao (122–148 km), Hengsha-Niupijiao (105–148 km), Niupijiao-Lvhua (148–195 km), and Hengsha-Lvhua (105–195 km) in 2007.

4. Results

4.1. Observed Decadal Tidal Evolution

In the South Branch, the 2-year averaged amplitude of M_2 tide from $x = 40$ km to $x = 0$ km is reduced by 12% in 1990–1991 whereas the reduction is only 3% in the periods 2009–2010 and 2019–2020 (Table S1). Conversely, the 2-year averaged amplitude of the M_4 overtide decreases by 1% from $x = 40$ km to $x = 0$ km in 1990%–1991% and 14% in the periods 2009–2010 and 2019–2020. As a result, the A_{M4}/A_{M2} amplitude ratio increased from 0.195 ($x = 40$ km) to 0.219 ($x = 0$ km) in 1990–1991 and decreased from 0.213 ($x = 40$ km) to 0.189 ($x = 0$ km) in 2009–2010. In 2019–2020, the A_{M4}/A_{M2} amplitude ratio decreased from 0.193 ($x = 40$ km) to 0.171 ($x = 0$ km). An increase and decrease in the A_{M4}/A_{M2} amplitude ratio implies more and less tidal distortion, respectively.

The damping factors and hydraulic head between $x = 0$ and $x = 40$ km are calculated for the three periods (1990–1991, 2009–2010, and 2019–2020, see Figure 4). The damping factors were overall smaller than 1, indicating predominantly landward damping. The mean damping factor was approximately 0.1 larger in the period 2009–2010 than 1990–1991 whereas the mean damping factor slightly decreased again from 2009–2010 to 2019–2020. Seasonal variations indicate a smaller damping factor under higher river discharge, which is more pronounced in 1990–1991 than the other two periods. Specifically, the damping factor in the dry season is ∼0.08 higher than in the wet season in 1990–1991. The hydraulic head also suggests significant seasonal variations in the three periods, that is, a larger hydraulic head under higher river discharge. From 1990–1991 to 2009–2010, the hydraulic head from $x = 0$ km to $x = 40$ km decreased, with an abrupt increase at the end of 2009 which is attributed to an increase in river discharge. From 2009–2010 to 2019–2020, the hydraulic head slightly increased.

The observed yearly averaged damping factors in the lower estuary (sections for $x > 60$ km) since 1997 are also provided per section (lines in Figures 5b and 5c). Unlike the weaker tidal damping in the South Branch (0–40 km), the damping factor in the South Channel (60–105 km) increased to 0.93 in 2004 and then decreased to 0.86 in 2011. In the North Passage (105–148 km), the observed damping was stronger from 1997 to ∼2005 followed by weakened damping afterward. Seaward of the North Passage (148–195 km), the damping factor (>1, tidal amplification) show similar variations as the North Passage with the lowest damping factor of 1.05 observed in 2006; although the damping factor decreased after 2010.
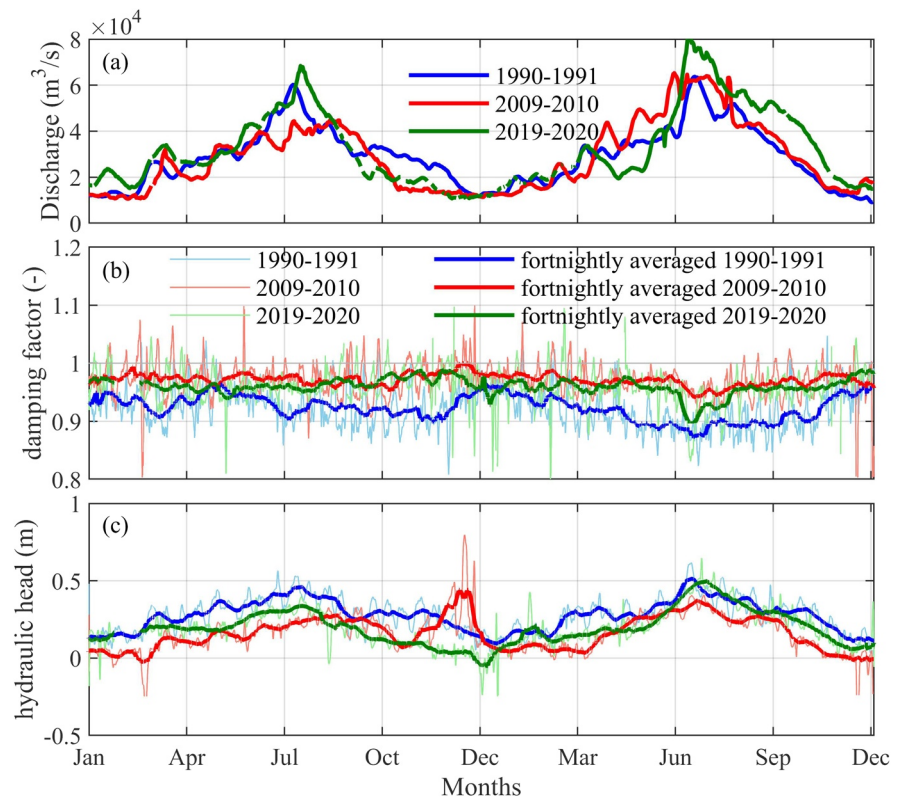
Figure 4. Variations of (a) river discharge at Datong, (b) damping factor and (c) hydraulic head between Xuliujing ($x = 0$ km) and Yanglin ($x = 40$ km) during 1990–1991, 2009–2010, and 2019–2020.

4.2. Computed Tidal Evolution

4.2.1. Historic Scenarios

The modeled tidal evolution ("tpg" series) over time is represented by the damping factors in different reaches in 1990, 1997, 2002, 2007, 2010, and 2020 (Figure 5b). In the South Branch (0–40 km), both the model results and observations suggest a decrease in tidal damping (~18% increase in the damping factor) from 1990 to 2010. However, the simulated change in tidal damping is ~13% larger than observations. In the lower estuary (all transects for $x > 60$ km), the simulated damping factor varies much less than the observed damping factors from 1997 to 2010. This suggests that tidal damping is less influenced by the topography, and therefore exemplified with more detailed comparisons of sections. In the South Channel (60–105 km), the modeled tidal damping is much lower than the observed damping. In the lower North Passage (122–148 km) and seaward of the North Passage (148–195 km), the modeled tidal damping is much stronger than the observed tidal damping.

Overall, in the South Branch, the observed and modeled tidal damping reasonably agree (reduced tidal damping), which is therefore primarily the result of topographic changes. Seaward of the South Branch, the observed and modeled changes disagree, implying that the tidal changes are less influenced by topographic changes. In the next section, we will explore the role of processes impacting the bed roughness (SSC, fluid mud) on tidal damping in more detail by varying the bed roughness in the model.

4.2.2. Changes in Bed Roughness

A local adjustment of the bed roughness only influences the regional damping factor (Figure 6a). A local 10% roughness reduction influences the damping factor more in regions A (2.1%) and B (2.5%) than in other regions (~1.7%). This sensitivity was used to develop a time- and spatial-varying roughness field with which
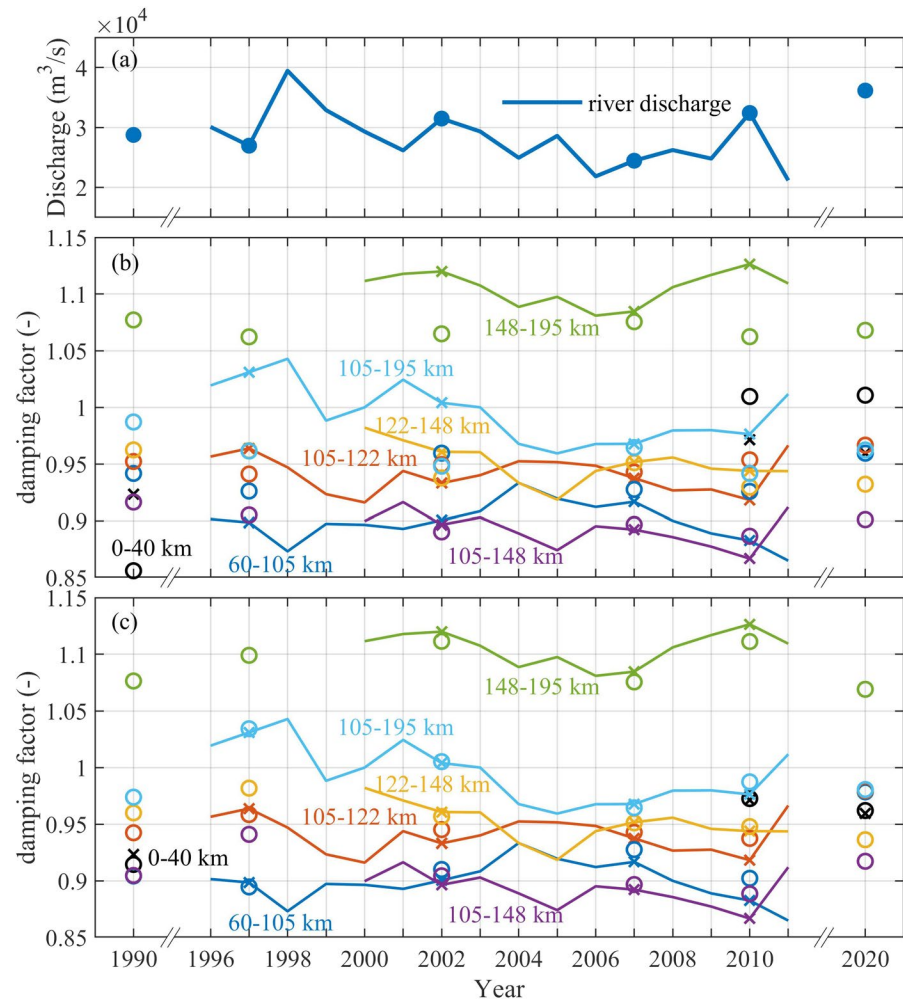
Figure 5. The yearly averaged (a) river discharge at Datong, (b) observed (solid lines for all years, crosses for years evaluated with the model) and computed ("tpg" series, circles) damping factors in the reaches Xuliujing-Yanglin (0–40 km), Shidongkou-Hengsha (60–105 km), Hengsha-Beicaozhong (105–122 km), Beicaozhong-Niupijiao (122–148 km), Hengsha-Niupijiao (105–148 km), Niupijiao-Lvhua (148–195 km), and Hengsha-Lvhua (105–195 km), and (c) same as (b) but the computed damping factors are from "cal_tpg" series with optimized roughness. Colors refer to the reach.

we recalibrated the numerical model (Figures 5c, 6c and 6d). The effect of local structures on the roughness change is estimated by comparing the differences in calibrated effective bottom roughness between simulations with local structures ("cal_tpg" series) and without local structures ("cal_mor" series) (Figure 6b). Specifically, the local structures mainly increase the roughness in the period of the construction, that is, a 30% increase in the roughness in region B from 1997 to 2002 and an 11% increase in regions D and E from 2002 to 2007. After 2002 in region C and after 2007 in regions D and E, the roughness decreased or remained relatively stable, which implies that the effects of the local structures are short-term. In region A, the effective bottom roughness shows a strong increase from 1990 to 2010 followed by a slight increase until 2020 (Figure 6c). Further seaward, the bed roughness varies more strongly over time (Figure 6d). The effective bottom roughness decreased by 6.7% in region E but increased by 60%, 9%, 60%, and 25% in regions A, B, C, and D, respectively from the 1990s to 2010. From 2010 to 2020, the effective bottom roughness slightly increased by 5% in region A.
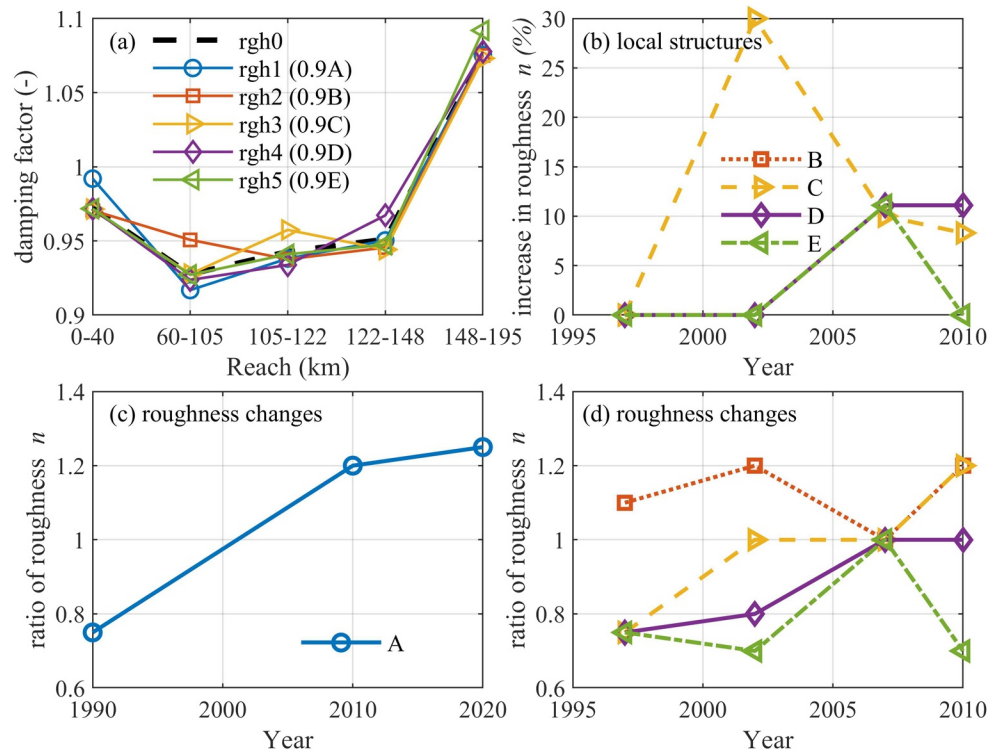
Figure 6. Modifications of the Manning coefficient n: (a) Model sensitivity to a 10% decrease in roughness ("rgh" series in Table 1) in the five regions-A, B, C, D, and E (see Figure 2), (b) the effect of simulated local structures on increasing the roughness, and changes in the effective bottom roughness in region A (c) and regions B, C, D, and E (d).

5. Discussion

5.1. Model Limitations: Effect of River Discharge

Given the changes in river discharge of the recent 30 years are limited, we assumed that variations in tidal damping are mainly attributed to changes in topography (morphology and local structures) and effective bottom roughness, but not to inter-annual river discharge changes. Note that the river discharge has changed at the seasonal time scales owing to dam constructions (L. Guo, Su, et al., 2018). To evaluate the effect of river discharge magnitude, we resolved the damping factors based on the M_2 amplitude using the s-tide function. The damping factors are further averaged during the periods when the river discharge is from 5,000 to 60,000 m^3/s with an increment of 5,000 m^3/s, for example, between 5,000 and 10,000 m^3/s, between 10,000 and 15,000 m^3/s. We see that the damping factor decreases with increasing river discharge in the reaches 0–40 km and 60–105 km (Figures 7a and 7b), but has negligible influence seaward of $x = 105$ km (Figures 7c and 7d). In the reach 0–40 km (South Branch), for equal river discharge, the damping factor in the period 1990–1991 is markedly lower than for the periods 2009–2010 and 2019–2020. This suggests that the impact of inter-annual changes in river discharge is much less important compared with the changes in morphology and bed roughness. The effect of river discharge is evaluated by rerunning the reference simulations with the river discharge of that particular year instead of using the 2007 hydrograph (as in the reference simulations). In the reaches 60–105, 105–148, and 148–195 km, no significant changes in damping factors are detected under the changes in seasonal variations among the years 1997, 2002, and 2010 compared to the year 2007. Therefore, it can be concluded that the dependence of the damping factor on river discharge is limited in the downstream reaches but more pronounced in the upper reaches. However, changes in morphology still dominate tidal damping in the reach 0–40 km.
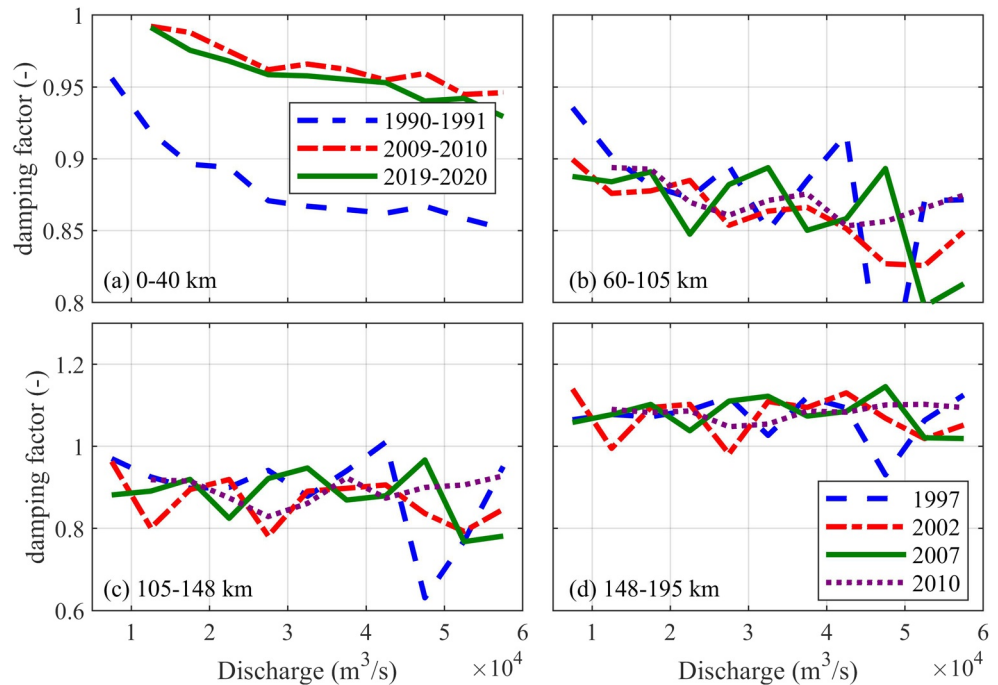
Figure 7. Observed damping factors (computed with nonstationary harmonic analysis) in the reach Xuliujing-Yanglin (0–40 km) with the river discharges measured at Datong during 1990–1991, 2009–2010, and 2019–2020 (a) and modeled damping factor in the reaches (b) Shidongkou-Hengsha (60–105 km), (c) Hengsha-Niupijiao (105–148 km) and (d) Niupijiao-Lvhua (148–195 km) with river discharges measured at Datong in 1997, 2002, 2007, and 2010 in the reference scenarios (see Table 1).
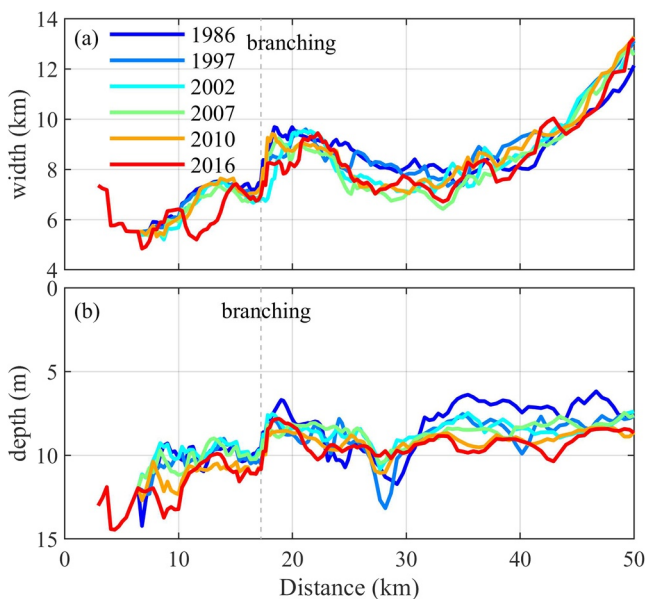
5.2. Effect of Morphological Changes

The morphological changes play a more important role in tidal damping in the reach 0–40 km (South Branch) than downstream of $x = 40$ km (Figure 5b). Therefore, we mainly explore the effect of morphological changes in the South Branch. The longitudinal variation in width and water depth is derived from bathymetries of the years 1986, 1997, 2002, 2007, 2010, and 2016 (Figure 8). The longitudinal change in width is defined by the cross-sectionally averaged width under the high and low water levels. Note that the high water level (1.37 m) and low water level (−1.32 m) for all years is based on Niupijiao station ($x = 148$ km) in the year 2007. The longitudinal changes of the water depth are defined as the cross-sectionally averaged depths below mean sea level (0 m).

From 1986 to 2010, the channel width decreased whereas the water depth increased. The increase in the water depth is primarily associated with the channel scouring caused by reduced riverine sediment supply since the mid-1980s (Y. Wang et al., 2013). The decrease in channel width may be ascribed to deposition in shallow areas and land reclamations (see Figure 2). Typically, both the decrease in width (strengthening the estuarine funnel shape) and increase in water depth weaken tidal damping (Dyer, 1997; Friedrichs & Aubrey, 1988, 1994; Jay, 1991; Savenije, 2006). However, the decrease in the hydraulic head cannot be explained by the decrease in the storage width, but only by the increase in depth. As a result, the reduced tidal damping in the South Branch (0–40 km) from 1990 to 2010 is primarily the result of the water depth increase. From 2010 to 2020, both the channel width and depth do not significantly change

Figure 8. Longitudinal changes of (a) cross-sectional averaged width between high and low water levels and (b) cross-sectional averaged water depth in 1986, 1997, 2002, 2007, 2010, and 2016. The "branching" indicates the location where the bifurcation between the North Branch and South Branch starts.

(Figure 8) and the modeled damping induced by the topography could not explain the slight decreasing damping factor (Figure 5). The decrease after 2010 is therefore more strongly influenced by the bed roughness, which will be discussed in the next section.

5.3. Mechanisms Responsible for Changes in Bed Roughness

We hypothesize that four factors may potentially influence the bed roughness, either through an increase (+), decrease (−) or both (see Table S2):

1. The construction of local structures (+).
2. The effect of the reduced riverine SSCs (+).
3. The formation of fluid mud (−).
4. The change of grain size of sediment (+) (−).

First, the construction of jetties and groins in the DCNP may increase hydraulic friction. These frictional effects are at least partly incorporated in the model (accounting for energy losses resulting from jetties and groins). However, local structures generate strong shear and vortices which enhance turbulence mixing (Ma et al., 2011). These small-scale hydrodynamic effects may not be well simulated in a model with mesh sizes not sufficiently small to represent these phenomena but can cause important frictional effects which require an increase in the prescribed bed roughness.

Second, the changing roughness over time may be related to the changes in SSC, that is, reduced hydraulic drag caused by the increase in the SSC (Winterwerp et al., 2009; Z. B. Wang et al., 2014). The riverine SSC has been decreasing since the mid-1980s and even more pronounced after 2003 (L. Guo, Su, et al., 2018; Luan et al., 2016; S. L. Yang et al., 2011; Zhao et al., 2018; C. Zhu et al., 2019). However, the changes of SSC in response to the reduced riverine SSC in the Yangtze Estuary are complex. Previous studies suggest that SSC has been decreasing in the South Branch since 2009 (W. Zhu et al., 2015) but remained unchanged in the South Channel and mouth zone (Dai et al., 2013; W. Zhu et al., 2015). H. Liu (2009) concluded that SSC in the South Branch and South Channel decreased and remained the same in the mouth zone but the assessment was based on 2-year observations only. We use five datasets of measured SSCs collected over similar periods (a spring-neap tidal cycle during the wet season), sampling methods, and locations in 2003, 2007, 2013, 2019, and 2020 (Figure 9). The observed tidally and depth-averaged SSC confirms a significant decreasing trend in the South Branch and South Channel from 2003 to 2013 and in the South Passage from 2003 to 2020, that is, reduced by 84%, 64%, and 63%, respectively. The SSC does not show a clear trend until 2013 in the North Channel, North Passage and the seaward areas whereas a 24% and 51% decrease in SSC was observed between 2013 and 2020 in the North Channel and North Passage, respectively. Seaward of the channels, the decrease in SSC is only pronounced in the two most recent years (2019–2020) with an average of reduction 46% among the three branches. Therefore, the reduced SSC is likely to cause an increase in effective bottom roughness in the South Branch and South Channel. However, within and seaward of the North Passage, the reduction in SSC was not large enough over the investigated period and therefore insufficiently to induce the changes in effective bottom roughness from 1997 to 2010. However, it is expected that the continued reduction in SSC will progressively more influence tidal propagation.

Third, the formation of fluid mud, which is a layer of near-bed high SSC, is extremely important in the suppression of turbulence, reducing roughness and strengthening tidal amplification (Allen et al., 1980; Gabioux et al., 2005). Fluid mud with a thickness of up to 1 m has been detected within and seaward of the North Passage since the 1970s (Li et al., 2001). After the construction of the DCNP, the thickness of the fluid mud in the North Passage was 1–5 m and was more frequently observed as a result of reinforced stratification in the narrowed and deepened channels (Lin et al., 2021; G. Liu et al., 2011; Song et al., 2013; Wan, Roelvink, et al., 2014). This is also consistent with the high siltation rate and large dredging demand in the regulated North Passage, triggering research on controlling mechanisms of the fluid mud (Jiang et al., 2013; Kuang et al., 2014; G. Liu et al., 2011; Wu et al., 2012). Therefore, enhanced fluid mud formation within and seaward of the North Passage has likely reduced the effective roughness.

Lastly, due to the upstream dam construction, the grain size of sediment may have changed in the Yangtze Estuary. The grain size of the suspended sediment has been reported to decrease, although varying with channels as well as hydrodynamic conditions (see Figure S2 adapted from Chen et al., 2016, 2019; Y. Yang
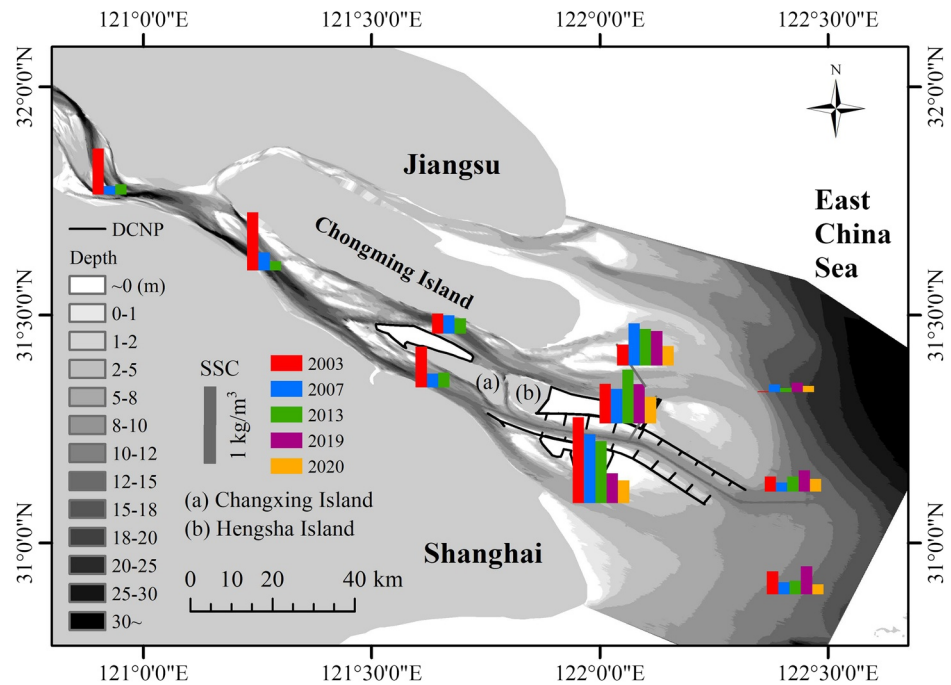
Figure 9. Tidal and depth-averaged suspended sediment concentrations (SSC) during the wet season in 2003, 2007, 2013, 2019, and 2020.

et al., 2016). The effect of the grain size of suspended sediment on roughness may be complex since the relationship between the two may be non-linear (van Maren, 2007). Very fine sediments are uniformly distributed over the water column and therefore have limited sediment-induced density effects (and therefore tidal dynamics). Similarly, very coarse sediment remains close to the bed, therefore also having a minor impact on sediment-induced density effects. Median grained sediment has the most pronounced effect on vertical stratification and through its impact on the vertical exchange of turbulent momentum and viscous dissipation on the apparent hydraulic roughness. It is likely that over decadal timescales, dams primarily reduce the flux of these medium-grained sediments to the Yangtze Estuary (van Maren et al., 2013). Additionally, the grain size of bed sediments affects roughness through skin friction, but even more through its impact on estuarine bed forms (form friction). The combined relationship between grain size and apparent roughness is therefore very complex. After the operation of the TGD in 2003, the grain size of bed sediments did not significantly change in the South Branch, South Channel and North Passage (Luo et al., 2012; Qiao, 2019), whereas coarsening of bed sediments was observed seaward of the North Passage (Luo et al., 2012, 2017; H. F. Yang et al., 2018; Zhan et al., 2020): the averaged median grain size of the bed sediments in the seaward area coarsened from 8.0 m in 1982 to 15.4 m in 2012 (H. F. Yang et al., 2018). Although we still insufficiently understand the effect of sediment grain size on roughness, observations suggest a change in grain size of the bed sediment and the suspended load, which may contribute to the changes in roughness.

The changes in effective bottom roughness and the potential effects of the various factors are illustrated in different regions (Figure 10). Note that we derive the changes in effective bottom roughness in the reaches for $x > 40$ km after 2010 based on the changes in damping factor from 2010 to 2011. In the South Branch, the 60% increase in roughness from 1990 to 2010 is mainly attributed to the strongly reduced SSC; the 5% increase after 2010 results from minor changes in SSC thereafter. Although the local structures were constructed in the North Passage, they may play a role in increasing the effective bottom roughness not only in the North Passage but also in its upstream (South Channel) and seaward area. The effect of local structures on raising the effective bottom roughness is also short-term (see the pronounced elevated bed roughness in the year 2002 in Figure 6b) and therefore such an effect may be limited after 2010. Moreover, the formation of fluid mud has been accelerated by the DCNP, which may play an increasing role in decreasing the effective bottom roughness in the North Passage and its seaward area. This effect may not strong enough to lead to a decrease in the effective bottom roughness in the North Passage during the DCNP construction
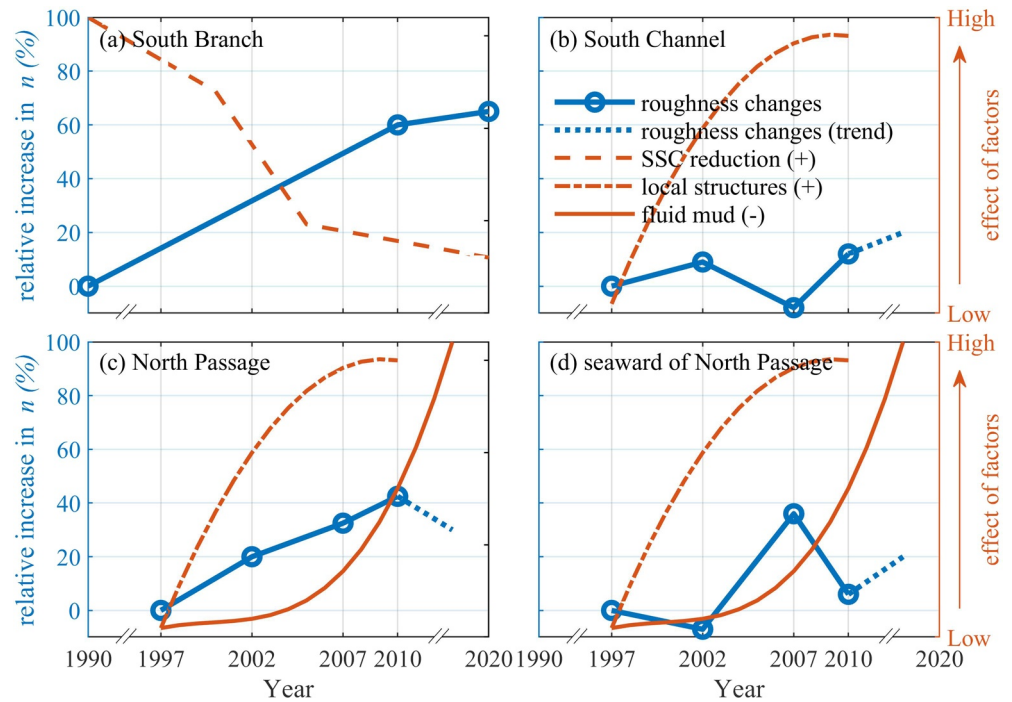
Figure 10. Sketch of the changing roughness (blue lines) in the (a) South Branch (region A), (b) South Channel (region B), (c) North Passage (regions C and D), and (d) seaward of the North Passage (region E) and the effects of the factors (red lines) on increasing (+) or decreasing (−) roughness. The factors include the reduction of suspended sediment concentrations (SSC), the construction of local structures from 1997 to 2010, and the increasing role of the fluid mud formation induced by the engineering works. The dashed blue lines indicate the increasing or decreasing trend of the roughness changes after 2010.

(1997–2010) but may contribute to the decrease in the effective bottom roughness after 2010. The grain size of suspended and bed sediments is influenced by the dam constructions and engineering works, which may either increase or decrease the roughness throughout the estuary.

5.4. Implications for Other Estuaries

Deepening and narrowing have resulted in profound tidal amplification in many estuaries (Talke & Jay, 2020; Winterwerp et al., 2013; Woodworth, 2010). In the South Branch of the Yangtze Estuary, changes in tides are mainly ascribed to riverine sediment decline rather than local engineering works, which is confirmed with the gradual changes in the damping factor from 2006 to 2015 (Figure S3). The reduced sediment supply may have two effects: (a) channel scouring (weakening tidal damping) and (b) reducing SSC and therefore increasing roughness (enhancing tidal damping). Sediment decline is a concern for the management of global deltas (e.g., Syvitski et al., 2009). In the South Branch, deepening and narrowing from 1990 to 2010 resulted in a predicted ~20% increase in the damping factor whereas the observed damping factor only increased ~5%. The ~75% contribution of deepening and narrowing on amplifying tides, that is, ~15% increase in damping factor, was therefore counteracted by the increase in the effective bottom roughness due to reduced SSC. Specifically, our model suggests a 60% increase in the effective bottom roughness in the South Branch from 1990 to 2010, which may correspond to the observed ~80% decrease in the SSC from 2003 to 2013. The effect of sediment decline on tidal damping is so large that it may be relevant for other highly concentrated estuaries as well. However, most estuaries in which tidal amplification has been well documented have concentrations that are either too low to significantly influence tidal dynamics (such as in the Venice Lagoon, see Ferrarin et al., 2015 and Cape Fear River estuary, see Familkhalili & Talke, 2016); or are declining, but at a rate insufficient to counterbalance deepening effects (the Hudson river estuary, see Ralston et al., 2019) or are increasing (Elbe, Ems, and Loire estuaries, see Winterwerp et al., 2013). In the Elbe, Ems, and Loir estuaries, a reduction in hydraulic roughness in response to increasing sediment

concentrations was also observed in response to deepening, leading to tidal amplification (Dijkstra, Schuttelaars, & Schramkowski, 2019; Dijkstra, Schuttelaars, Schramkowski, & Brouwer, 2019; Jalón-Rojas et al., 2016; van Maren et al., 2015; Winterwerp et al., 2013). Moreover, a positive feedback between tidal amplification and an increase in SSC may occur in these estuaries (Winterwerp & Wang, 2013; Winterwerp et al., 2013). However, these western European estuaries are examples of systems with a primarily marine source of sediment. Therefore, the change of tidal damping in the South Branch with a fluvial sediment source does not influence the SSC.

On the other hand, the tidal evolution in the mouth zone is controlled by the local engineering works which initially led to an increase in the effective bottom roughness, but later to a decrease as they also strengthened fluid mud formation. The fluid mud is likely to decrease the effective bottom roughness after 2010, resulting in less tidal damping, which is similar to the Elbe, Ems, and Loir estuaries. However, the changes in tides in the mouth zone were overall small in magnitude, which may not be strong enough to induce changes in SSC, particularly considering that the riverine sediment decline is prone to reduce the SSC. Such an effect in the mouth zone of the Yangtze Estuary may need future research.

6. Conclusions

The tides in many estuaries are changing in response to natural and human factors operating concurrently. In this work, we analyzed the tidal evolution in the Yangtze Estuary from the 1990s to 2020 using damping factors. Data analysis in the South Branch suggests a strong decrease in landward tidal damping from 1990 to 2010, but a minor increase in landward tidal damping from 2010 to 2020. Tidal damping increased in the mouth zone from 1997 to 2010.

A calibrated 2D hydrodynamic model is then used to investigate the effects of morphological changes, local structures and roughness. We found that reduced sediment supply controls the reduced tidal damping in the South Branch. Specifically, the tides are amplified primarily due to the increase in water depth (channel scouring). However, we also estimate that the ~80% reduction in SSC has increased the effective bottom roughness (represented with a Manning coefficient) by 60%. This enhanced bed roughness reduces tidal damping, counteracting the impact of scouring by a reduced sediment supply on tidal amplification by ~75%. In the mouth zone, the effective bottom roughness overall increased until 2010, which is mainly attributed to the effects of local structures and partly counteracted by fluid mud formation. Fluid mud decreases the effective bed roughness, therefore weakening tidal damping after 2010. However, around the same period, the SSC declined, generating an opposite effect on apparent bed roughness and tidal damping. The changes in sediment grain size may also influence to some extent, either increasing or decreasing the apparent hydraulic roughness, adapting to both reduced sediment supply and local engineering works.

In conclusion, the tides in the Yangtze estuary responded to various human interventions on a local scale (fairway construction, land reclamations) and a larger scale (sediment load reduction). These interventions have influenced tidal dynamics through the impact on morphology (deepening) and roughness (involving complex feedback mechanism between hydrodynamics, sediment concentration and grain size, and fluid mud formation). As a result of the large number of mechanisms involved in spatial- and temporal-varying tidal damping, understanding the impact of such mechanisms on decadal tidal evolution is important for the management of turbid estuaries in general, exemplified in this study with the Yangtze Estuary.

Data Availability Statement

Data were collected from the websites of the bureau of Hydrology, Changjiang Water Resources Commission (http://www.cjh.com.cn), the open-accessed bulletins published by the Ministry of Water Resources of China (http://www.mwr.gov.cn/sj/tjgb/zghlnsgb/), and the Hydro-information Centre of the Ministry of Water Resources of Jiangsu Province (http://221.226.28.67:88/jsswxxSSI/Web/Default.html?m=2). Data used in this study are publicly available at https://figshare.com/s/50a773714c3354eab710.

References

Allen, G. P., Salomon, J., Bassoullet, P., Du Penhoat, Y., & De Grandpre, C. (1980). Effects of tides on mixing and suspended sediment transport in macrotidal estuaries. *Sedimentary Geology*, *26*(1–3), 69–90. https://doi.org/10.1016/0037-0738(80)90006-8

Araújo, I., Dias, J., & Pugh, D. (2008). Model simulations of tidal changes in a coastal lagoon, the Ria de Aveiro (Portugal). *Continental Shelf Research*, *28*(8), 1010–1025. https://doi.org/10.1016/j.csr.2008.02.001

Cai, H., Savenije, H., & Toffolon, M. (2014). Linking the river to the estuary: Influence of river discharge on tidal damping. *Hydrology and Earth System Sciences*, *18*(1), 287–304. https://doi.org/10.5194/hess-18-287-2014

Chen, Y., He, Q., Zhang, D., & Guo, C. (2016). Grain size distribution of suspended sediment in Yangtze River Estuary turbidity maximum in dry season. *Journal of Sediment Research*, *1*, 24–30. (in Chinese with Abstract in English).

Chen, Y., He, Q., Zhang, Y., & Lin, J. (2019). Grain size distribution of suspended sediment in Yangtze River Estuary turbidity maximum in wet season. *Journal of Sediment Research*, *5*, 48–55. (in Chinese with Abstract in English).

Cheng, Z., Jalon-Rójas, I., Wang, X. H., & Liu, Y. (2020). Impacts of land reclamation on sediment transport and sedimentary environment in a macro-tidal estuary. *Estuarine, Coastal and Shelf Science*, *242*, 106861. https://doi.org/10.1016/j.ecss.2020.106861

Dai, Z.-J., Chu, A., Li, W.-H., Li, J.-F., & Wu, H.-L. (2013). Has suspended sediment concentration near the mouth bar of the Yangtze (Changjiang) estuary been declining in recent years? *Journal of Coastal Research*, *289*, 809–818. https://doi.org/10.2112/jcoastres-d-11-00200.1

de Jonge, V. N., Schuttelaars, H. M., van Beusekom, J. E. E., Talke, S. A., & de Swart, H. E. (2014). The influence of channel deepening on estuarine turbidity levels and dynamics, as exemplified by the Ems Estuary. *Estuarine, Coastal and Shelf Science*, *139*, 46–59. https://doi.org/10.1016/j.ecss.2013.12.030

Dijkstra, Y. M., Schuttelaars, H. M., & Schramkowski, G. P. (2019). A regime shift from low to high sediment concentrations in a tide-dominated estuary. *Geophysical Research Letters*, *46*(8), 4338–4345. https://doi.org/10.1029/2019gl082302

Dijkstra, Y. M., Schuttelaars, H. M., Schramkowski, G. P., & Brouwer, R. L. (2019). Modeling the transition to high sediment concentrations as a response to channel deepening in the Ems River Estuary. *Journal of Geophysical Research: Oceans*, *124*(3), 1578–1594. https://doi.org/10.1029/2018jc014367

Dyer, K. R. (1997). *Estuaries: A physical introduction* (2nd ed.). John Wiley Sons.

Familkhalili, R., & Talke, S. A. (2016). The effect of channel deepening on tides and storm surge: A case study of Wilmington, nc. *Geophysical Research Letters*, *43*(17), 9138–9147. https://doi.org/10.1002/2016gl069494

Ferrarin, C., Tomasin, A., Bajo, M., Petrizzo, A., & Umgiesser, G. (2015). Tidal changes in a heavily modified coastal wetland. *Continental Shelf Research*, *101*, 22–33. https://doi.org/10.1016/j.csr.2015.04.002

Friedrichs, C. T., & Aubrey, D. G. (1988). Non-linear tidal distortion in shallow well-mixed estuaries—A synthesis. *Estuarine, Coastal and Shelf Science*, *27*(5), 521–545. https://doi.org/10.1016/0272-7714(88)90082-0

Friedrichs, C. T., & Aubrey, D. G. (1994). Tidal propagation in strongly convergent channels. *Journal of Geophysical Research*, *99*(C2), 3321. https://doi.org/10.1029/93jc03219

Fu, G. (2013). Recent changes of tidal characteristics in the Yangtze Estuary. *Port and Waterway Engineering*, *11*, 61–69. (Chinese with Abstract in English).

Gabioux, M., Vinzon, S. B., & Paiva, A. M. (2005). Tidal propagation over fluid mud layers on the amazon shelf. *Continental Shelf Research*, *25*(1), 113–125. https://doi.org/10.1016/j.csr.2004.09.001

Geyer, W. R. (1993). The importance of suppression of turbulence by stratification on the estuarine turbidity maximum. *Estuaries*, *16*(1), 113. https://doi.org/10.2307/1352769

Grasso, F., & Le Hir, P. (2019). Influence of morphological changes on suspended sediment dynamics in a macrotidal estuary: Diachronic analysis in the Seine Estuary (France) from 1960 to 2010. *Ocean Dynamics*, *69*(1), 83–100. https://doi.org/10.1007/s10236-018-1233-x

Guo, L., Su, N., Zhu, C., & He, Q. (2018). How have the river discharges and sediment loads changed in the Changjiang River basin downstream of the Three Gorges Dam? *Journal of Hydrology*, *560*, 259–274. https://doi.org/10.1016/j.jhydrol.2018.03.035

Guo, L., van der Wegen, M., Jay, D. A., Matte, P., Wang, Z. B., Roelvink, D., & He, Q. (2015). River-tide dynamics: Exploration of nonstationary and nonlinear tidal behavior in the Yangtze River Estuary. *Journal of Geophysical Research: Oceans*, *120*(5), 3499–3521. https://doi.org/10.1002/2014jc010491

Guo, W., Wang, X. H., Ding, P., Ge, J., & Song, D. (2018). A system shift in tidal choking due to the construction of Yangshan Harbour, Shanghai, China. Estuarine. *Coastal and Shelf Science*, *206*, 49–60. https://doi.org/10.1016/j.ecss.2017.03.017

Hu, K., & Ding, P. (2009). The effect of deep waterway constructions on hydrodynamics and salinities in Yangtze Estuary, China. *Journal of Coastal Research*, 961–965.

Hu, K., Ding, P., Wang, Z., & Yang, S. (2009). A 2D/3D hydrodynamic and sediment transport model for the Yangtze Estuary, China. *Journal of Marine Systems*, *77*(1–2), 114–136. https://doi.org/10.1016/j.jmarsys.2008.11.014

Jalón-Rojas, I., Schmidt, S., Sottolichio, A., & Bertier, C. (2016). Tracking the turbidity maximum zone in the Loire Estuary (France) based on a long-term, high-resolution and high-frequency monitoring network. *Continental Shelf Research*, *117*, 1–11. https://doi.org/10.1016/j.csr.2016.01.017

Jalón-Rojas, I., Sottolichio, A., Hanquiez, V., Fort, A., & Schmidt, S. (2018). To what extent multidecadal changes in morphology and fluvial discharge impact tide in a convergent (turbid) tidal river. *Journal of Geophysical Research: Oceans*, *123*(5), 3241–3258.

Jay, D. A. (1991). Green's law revisited: Tidal long-wave propagation in channels with strong topography. *Journal of Geophysical Research*, *96*(C11), 20585–20598. https://doi.org/10.1029/91jc01633

Jay, D. A., Leffler, K., & Degens, S. (2011). Long-term evolution of Columbia River tides. *Journal of Waterway, Port, Coastal, and Ocean Engineering*, *137*(4), 182–191. https://doi.org/10.1061/(asce)ww.1943-5460.0000082

Jiang, C., de Swart, H. E., Li, J., & Liu, G. (2013). Mechanisms of along-channel sediment transport in the North Passage of the Yangtze Estuary and their response to large-scale interventions. *Ocean Dynamics*, *63*(2–3), 283–305. https://doi.org/10.1007/s10236-013-0594-4

Jiang, C., Li, J., & de Swart, H. E. (2012). Effects of navigational works on morphological changes in the bar area of the Yangtze Estuary. *Geomorphology*, *139–140*, 205–219. https://doi.org/10.1016/j.geomorph.2011.10.020

Kuang, C.-P., Chen, W., Gu, J., & He, L.-l. (2014). Comprehensive analysis on the sediment siltation in the upper reach of the deepwater navigation channel in the Yangtze Estuary. *Journal of Hydrodynamics*, *26*(2), 299–308. https://doi.org/10.1016/s1001-6058(14)60033-0

Kukulka, T., & Jay, D. A. (2003). Impacts of Columbia River discharge on salmonid habitat: 1. A nonstationary fluvial tide model. *Journal of Geophysical Research: Oceans*, *108*(C9). https://doi.org/10.1029/2002jc001382

Lesser, G. R., Roelvink, J. A., van Kester, J. A. T. M., & Stelling, G. S. (2004). Development and validation of a three-dimensional morphological model. *Coastal Engineering*, *51*(8–9), 883–915. https://doi.org/10.1016/j.coastaleng.2004.07.014

Li, J., He, Q., Xiang, W., Wan, X., & Shen, H. (2001). Fluid mud transportation at water wedge in the Changjiang Estuary. *Science in China, Series B: Chemistry*, *44*(1), 47–56. https://doi.org/10.1007/bf02884808

Lin, J., van Prooijen, B. C., Guo, L., Zhu, C., He, Q., & Wang, Z. B. (2021). Regime shifts in the Changjiang (Yangtze River) Estuary: The role of concentrated benthic suspensions. *Marine Geology*, *433*, 106403. https://doi.org/10.1016/j.margeo.2020.106403

Liu, G., Zhu, J., Wang, Y., Wu, H., & Wu, J. (2011). Tripod measured residual currents and sediment flux: Impacts on the silting of the Deep-water Navigation Channel in the Changjiang Estuary. *Estuarine, Coastal and Shelf Science*, *93*(3), 192–201. https://doi.org/10.1016/j.ecss.2010.08.008

Liu, H. (2009). *Sediment mixing and exchange processes in the Yangtze Estuary*. (Thesis). East China Normal University.

Lopes, C. L., Plecha, S., Silva, P. A., & Dias, J. M. (2013). Influence of morphological changes in a lagoon flooding extension: Case study of Ria de Aveiro (Portugal). *Journal of Coastal Research*, *65*(sp2), 1158–1163. https://doi.org/10.2112/si65-196.1

Lu, S., Tong, C., Lee, D.-Y., Zheng, J., Shen, J., Zhang, W., & Yan, Y. (2015). Propagation of tidal waves up in Yangtze Estuary during the dry season. *Journal of Geophysical Research: Oceans*, *120*(9), 6445–6473. https://doi.org/10.1002/2014jc010414

Luan, H. L., Ding, P. X., Wang, Z. B., Ge, J. Z., & Yang, S. L. (2016). Decadal morphological evolution of the Yangtze Estuary in response to river input changes and estuarine engineering projects. *Geomorphology*, *265*, 12–23. https://doi.org/10.1016/j.geomorph.2016.04.022

Luo, X. X., Yang, S. L., Wang, R. S., Zhang, C. Y., & Li, P. (2017). New evidence of Yangtze Delta recession after closing of the three gorges dam. *Scientific Reports*, *7*, 41735. https://doi.org/10.1038/srep41735

Luo, X. X., Yang, S. L., & Zhang, J. (2012). The impact of the Three Gorges Dam on the downstream distribution and texture of sediments along the middle and lower Yangtze River (Changjiang) and its estuary, and subsequent sediment dispersal in the East China Sea. *Geomorphology*, *179*, 126–140. https://doi.org/10.1016/j.geomorph.2012.05.034

Ma, G., Shi, F., Liu, S., & Qi, D. (2011). Hydrodynamic modeling of Changjiang Estuary: Model skill assessment and large-scale structure impacts. *Applied Ocean Research*, *33*(1), 69–78. https://doi.org/10.1016/j.apor.2010.10.004

Matte, P., Jay, D. A., & Zaron, E. D. (2013). Adaptation of classical tidal harmonic analysis to nonstationary tides, with application to river tides. *Journal of Atmospheric and Oceanic Technology*, *30*(3), 569–589. https://doi.org/10.1175/jtech-d-12-00016.1

Pan, H., Lv, X., Wang, Y., Matte, P., Chen, H., & Jin, G. (2018). Exploration of tidal-fluvial interaction in the Columbia River estuary using s_tide. *Journal of Geophysical Research: Oceans*, *123*(9), 6598–6619. https://doi.org/10.1029/2018jc014146

Pawlowicz, R., Beardsley, B., & Lentz, S. (2002). Classical tidal harmonic analysis including error estimates in matlab using t-tide. *Computers & Geosciences*, *28*(8), 929–937. https://doi.org/10.1016/S0098-3004(02)00013-4

Qiao, Y. (2019). *Erodibility of bed sediments in the Yangtze Estuary*. (Unpublished master's thesis). East China Normal University.

Ralston, D. K., Talke, S., Geyer, W. R., Al-Zubaidi, H. A., & Sommerfield, C. K. (2019). Bigger tides, less flooding: Effects of dredging on barotropic dynamics in a highly modified estuary. *Journal of Geophysical Research: Oceans*, *124*(1), 196–211. https://doi.org/10.1029/2018jc014313

Savenije, H. H. (2006). *Salinity and tides in alluvial estuaries*. Elsevier.

Song, D., Wang, X. H., Cao, Z., & Guan, W. (2013). Suspended sediment transport in the deepwater navigation channel, Yangtze River Estuary, China, in the dry season 2009: 1. Observations over spring and neap tidal cycles. *Journal of Geophysical Research: Oceans*, *118*(10), 5555–5567. https://doi.org/10.1002/jgrc.20410

Syvitski, J. P., Kettner, A. J., Overeem, I., Hutton, E. W., Hannon, M. T., Brakenridge, G. R., et al. (2009). Sinking deltas due to human activities. *Nature Geoscience*, *2*(10), 681–686. https://doi.org/10.1038/ngeo629

Talke, S. A., & Jay, D. A. (2020). Changing tides: The role of natural and anthropogenic factors. *Annual Review of Marine Science*, *12*, 121–151. https://doi.org/10.1146/annurev-marine-010419-010727

van Maren, D. S. (2007). Grain size and sediment concentration effects on channel patterns of silt-laden rivers. *Sedimentary Geology*, *202*(1–2), 297–316. https://doi.org/10.1016/j.sedgeo.2007.04.001

van Maren, D. S., Winterwerp, J. C., & Vroom, J. (2015). Fine sediment transport into the hyper-turbid lower ems river: The role of channel deepening and sediment-induced drag reduction. *Ocean Dynamics*, *65*(4), 589–605. https://doi.org/10.1007/s10236-015-0821-2

van Maren, D. S., Yang, S.-L., & He, Q. (2013). The impact of silt trapping in large reservoirs on downstream morphology: The Yangtze River. *Ocean Dynamics*, *63*(6), 691–707. https://doi.org/10.1007/s10236-013-0622-4

Vellinga, N., Hoitink, A., van der Vegt, M., Zhang, W., & Hoekstra, P. (2014). Human impacts on tides overwhelm the effect of sea level rise on extreme water levels in the Rhine–Meuse delta. *Coastal Engineering*, *90*, 40–50. https://doi.org/10.1016/j.coastaleng.2014.04.005

Wan, Y., Gu, F., Wu, H., & Roelvink, D. (2014). Hydrodynamic evolutions at the Yangtze Estuary from 1998 to 2009. *Applied Ocean Research*, *47*, 291–302. https://doi.org/10.1016/j.apor.2014.06.009

Wan, Y., Roelvink, D., Li, W., Qi, D., & Gu, F. (2014). Observation and modeling of the storm-induced fluid mud dynamics in a muddy-estuarine navigational channel. *Geomorphology*, *217*, 23–36. https://doi.org/10.1016/j.geomorph.2014.03.050

Wang, D., Pan, H., Jin, G., & Lv, X. (2020). Seasonal variation of the principal tidal constituents in the Bohai Sea. *Ocean Science*, *16*(1), 1–14. https://doi.org/10.5194/os-16-1-2020

Wang, Y., Dong, P., Oguchi, T., Chen, S., & Shen, H. (2013). Long-term (1842–2006) morphological change and equilibrium state of the Changjiang (Yangtze) Estuary, China. *Continental Shelf Research*, *56*, 71–81. https://doi.org/10.1016/j.csr.2013.02.006

Wang, Z. B., Vandenbruwaene, W., Taal, M., & Winterwerp, H. (2019). Amplification and deformation of tidal wave in the Upper Scheldt Estuary. *Ocean Dynamics*, *69*(7), 829–839. https://doi.org/10.1007/s10236-019-01281-3

Wang, Z. B., Winterwerp, J. C., & He, Q. (2014). Interaction between suspended sediment and tidal amplification in the Guadalquivir Estuary. *Ocean Dynamics*, *64*(10), 1487–1498. https://doi.org/10.1007/s10236-014-0758-x

Winterwerp, J. C. (2001). Stratification effects by cohesive and noncohesive sediment. *Journal of Geophysical Research*, *106*(C10), 22559–22574. https://doi.org/10.1029/2000jc000435

Winterwerp, J. C. (2011). Fine sediment transport by tidal asymmetry in the high-concentrated Ems River: Indications for a regime shift in response to channel deepening. *Ocean Dynamics*, *61*(2–3), 203–215. https://doi.org/10.1007/s10236-010-0332-0

Winterwerp, J. C., Lely, M., & He, Q. (2009). Sediment-induced buoyancy destruction and drag reduction in estuaries. *Ocean Dynamics*, *59*(5), 781–791. https://doi.org/10.1007/s10236-009-0237-y

Winterwerp, J. C., & Wang, Z. B. (2013). Man-induced regime shifts in small estuaries—I: Theory. *Ocean Dynamics*, *63*(11–12), 1279–1292. https://doi.org/10.1007/s10236-013-0662-9

Winterwerp, J. C., Wang, Z. B., van Braeckel, A., van Holland, G., & Kösters, F. (2013). Man-induced regime shifts in small estuaries—II: A comparison of rivers. *Ocean Dynamics*, *63*(11–12), 1293–1306. https://doi.org/10.1007/s10236-013-0663-8

Woodworth, P. (2010). A survey of recent changes in the main components of the ocean tide. *Continental Shelf Research*, *30*(15), 1680–1691. https://doi.org/10.1016/j.csr.2010.07.002

Wu, J., Liu, J. T., & Wang, X. (2012). Sediment trapping of turbidity maxima in the Changjiang Estuary. *Marine Geology*, *303–306*, 14–25. https://doi.org/10.1016/j.margeo.2012.02.011

Yang, H. F., Yang, S. L., Meng, Y., Xu, K. H., Luo, X. X., Wu, C. S., & Shi, B. W. (2018). Recent coarsening of sediments on the southern Yangtze subaqueous delta front: A response to river damming. *Continental Shelf Research*, *155*, 45–51. https://doi.org/10.1016/j.csr.2018.01.012

Yang, S. L., Milliman, J. D., Li, P., & Xu, K. (2011). 50,000 dams later: Erosion of the Yangtze River and its delta. *Global and Planetary Change*, *75*(1–2), 14–20. https://doi.org/10.1016/j.gloplacha.2010.09.006

Yang, Y., Zhang, M., Fan, Y., Li, Y., & Liu, W. (2016). Variation trend and causes of suspended sediment characteristic in Yangtze Estuary. *Journal of Basic Science and Engineering*, *6*, 48–55. (in Chinese with Abstract in English).

Yun, C. (2004). *Recent development of the Changjiang Estuary*.

Zhan, Q., Li, M., Liu, X., Chen, J., & Chen, Z. (2020). Sedimentary transition of the Yangtze subaqueous delta during the past century: Inspiration for delta response to future decline of sediment supply. *Marine Geology*, *428*, 106279. https://doi.org/10.1016/j.margeo.2020.106279

Zhao, J., Guo, L., He, Q., Wang, Z. B., van Maren, D. S., & Wang, X. (2018). An analysis on half century morphological changes in the Changjiang Estuary: Spatial variability under natural processes and human intervention. *Journal of Marine Systems*, *181*, 25–36. https://doi.org/10.1016/j.jmarsys.2018.01.007

Zhu, C., Guo, L., van Maren, D. S., Tian, B., Wang, X., He, Q., & Wang, Z. B. (2019). Decadal morphological evolution of the mouth zone of the Yangtze Estuary in response to human interventions. *Earth Surface Processes and Landforms*, *44*(12), 2319–2332. https://doi.org/10.1002/esp.4647

Zhu, J., Weisberg, R. H., Zheng, L., & Han, S. (2015). Influences of channel deepening and widening on the tidal and nontidal circulations of Tampa Bay. *Estuaries and Coasts*, *38*(1), 132–150. https://doi.org/10.1007/s12237-014-9815-4

Zhu, L., He, Q., & Shen, J. (2018). Modeling lateral circulation and its influence on the along-channel flow in a branched estuary. *Ocean Dynamics*, *68*(2), 177–191. https://doi.org/10.1007/s10236-017-1114-8

Zhu, L., He, Q., Shen, J., & Wang, Y. (2016). The influence of human activities on morphodynamics and alteration of sediment source and sink in the Changjiang estuary. *Geomorphology*, *273*, 52–62. https://doi.org/10.1016/j.geomorph.2016.07.025

Zhu, W., Li, J., & Sanford, L. P. (2015). Behavior of suspended sediment in the Changjiang Estuary in response to reduction in river sediment supply. *Estuaries and Coasts*, *38*(6), 2185–2197. https://doi.org/10.1007/s12237-014-9929-8